

Effects of Charge and Gravitational Decoupling on Complexity and Isotropization of Anisotropic Models

M. Sharif¹ *and Tayyab Naseer^{1,2} †

¹ Department of Mathematics and Statistics, The University of Lahore,
1-KM Defence Road Lahore-54000, Pakistan.

² Department of Mathematics, University of the Punjab,
Quaid-i-Azam Campus, Lahore-54590, Pakistan.

Abstract

This paper constructs two immediate extensions of the existing anisotropic solutions in the context of Einstein-Maxwell framework by employing minimal geometric deformation. To achieve this, we assume a static spherical interior initially filled with anisotropic fluid and call it a seed source. We extend this matter configuration by including a new source whose impact on the self-gravitating system is governed by a decoupling parameter. The charged field equations analogous to the total fluid source are formulated. We then implement a transformation on the radial metric potential that divides the field equations into two new under-determined systems, corresponding to the initial and new sources. The first of them is addressed by taking two well-known metric ansatz so that the number of unknowns can be tackled. Further, the vanishing of total anisotropy and complexity-free constraints are used to solve the second set. The estimated radius and mass of a compact star $4U\ 1820 - 30$ is utilized to interpret the resulting solutions graphically for different values of the charge and decoupling parameter ω . We conclude that our both developed models are physically acceptable for all parametric values except $\omega = 1$.

*msharif.math@pu.edu.pk

†tayyabnaseer48@yahoo.com

Keywords: Geometric deformation; Anisotropy; Self-gravitating system.
PACS: 04.20.Jb; 95.36.+x.

1 Introduction

General theory of relativity (GR) has gained significant acceptance throughout the scientific community as it is considered the most desirable tool for understanding the nature of gravitational field. This theory relates the matter configuration with the geometry of a spacetime structure characterized by the energy-momentum tensor (EMT) and the Einstein tensor, respectively through Einstein's field equations. The exact/numerical formulation of their solutions has become an interesting topic among physicists through which they study the structural properties of self-gravitating systems. Schwarzschild pioneered this work by calculating the analytical solution of such equations that prompted researchers to extend this in the context of GR and other modified theories. For the first time in 1916, he started with the assumption of a spherical geometry possessing uniform density and formulated the corresponding exterior [1] and interior solutions [2]. The literature offers a large number of solutions in recent times describing geometrical structures coupled with different fluid distributions.

Among all solutions of the field equations, those which can be used to model physically acceptable compact bodies have made remarkable achievements in the literature. However, it is rather difficult to calculate such solutions because the field equations involve multiple geometric terms that make them highly non-linear. Such non-linearity forced researchers to develop certain approaches which can be used to solve these equations and produce physically relevant results. The novel and innovative strategy among them is the gravitational decoupling which is empowered to tackle with several factors reigning the interior distribution such as anisotropy, dissipation flux, expansion scalar and shear, etc. This technique leads the field equations in a new reference frame where each fluid source is characterized by an individual system of equations, and hence, each set can be solved easily. Further, decoupling offers two different types, namely minimal (MGD) and extended geometric deformations, transforming radial and both temporal/radial metric potentials, respectively.

Ovalle [3] recently pioneered the MGD scheme in the braneworld (BW) scenario and discussed compact objects characterized by exact solutions. Fol-

lowing this, Ovalle and Linares [4] assumed Tolman IV spacetime as the isotropic solution and developed its corresponding anisotropic analog in the context of BW through the same technique. The study of different phenomena have been made possible through this technique, such as the derivation of solutions corresponding to spherical [5] interior, originating acceptable inner fluid solution [6, 7], studying microscopic properties of black holes [8, 9] and discussing the impact of Weyl stresses [10]. The perturbation was applied to the field equations in BW and bulk, and results were found compatible with each other [11]-[15]. The MGD technique was then extended by transforming both g_{tt} and g_{rr} metric coefficients of a static sphere to obtain a modified form of the Schwarzschild geometry in BW [16].

Initially, a self-gravitating geometry was considered to be coupled with the isotropic fluid in which the pressure acts the same in each direction, usually radial and tangential. However, the pioneering work by Jeans made some revolutions in the literature, suggesting that anisotropy may occur in the interior due to the presence of multiple factors [17]. A theoretical analysis has been done by Ruderman [18] from which he found that the heavily stellar models (i.e., with energy density not less than 10^{15} g/cm^3) may possess anisotropy. A compact star surrounded by a high magnetic field [19]-[22] as well as certain other elements [23]-[25] must contain anisotropy in its interior. Ovalle et al. [26] considered that a spherical fluid and Schwarzschild vacuum spacetime do not exchange energy and momentum with each other, and developed a new anisotropic solution by using MGD approach. Anisotropic extensions to different isotropic models such as Heintzmann, Duragpal-Fuloria and Tolman VII spacetimes have also been obtained [27]-[29]. Sharif and his collaborators [30, 31] have done the same analysis for charged/uncharged spacetimes in GR as well as different extended theories and found acceptable results. We have developed physically relevant anisotropic compact models in a non-minimally coupled gravity for certain values of the corresponding parameters [32].

The inclusion of the electric charge has a significant role in the study of compact structures. Electromagnetic forces are considered as the most significant ingredients that help to to reduce the attractive force of gravity. Therefore, a sufficiently enough amount of the charge is needed to resist the gravitational force and hence, the stability of a star is preserved. Bekenstein [33] considered a dynamical spherical model coupled with the electromagnetic field and deduced that the force produced by the charge has repulsive behavior, helping the geometry to maintain its stability. This work has been

extended by Esculpi and Aloma [34] for the case of anisotropic fluid from which they observed that both positive anisotropy and charge have repulsive effects. The structure of anisotropic charged stars has been studied by taking a power-law interior charge distribution in terms of exterior charge and radius of the considered compact object, and physically relevant results were obtained [35, 36]. Maurya et al. [37] analyzed the interior distribution of charged stellar models configured with the baryonic fluid via the Karmarkar condition. They solved the corresponding Einstein-Maxwell field equations and observed the resulting matter variables to be dependent on the electromagnetic field.

Herrera [38] recently developed a new definition of the complexity for a static sphere that encounters the factors which complicate the system. Initially, Bel decomposed the curvature tensor into its orthogonal components and found certain scalars, named the structure scalars. Herrera adopted the same formulation for anisotropic fluid to obtain the corresponding scalars that were appeared to be associated with different physical parameters. One of those scalars possesses both anisotropy and inhomogeneous density, came up with his criteria and thus named as the complexity factor. Such a definition has been observed highly acceptable in every field of science. Herrera et al. [39] used this definition to discuss the evolutionary patterns for dynamical dissipative geometry. Yousaf et al. [40, 41] performed the same analysis in a particular non-minimal theory and examined the impact of modified gravity on charged/uncharged spheres and cylinders. The complexity-free models can be obtained once we substitute the corresponding complexity factor equals to zero. This constraint has been employed to static self-gravitating spheres, and several physically relevant objects are modeled [42]-[46].

This article extends the anisotropic spherical solutions to the Einstein-Maxwell framework through the MGD technique. To do this work, we follow the structure defined in the succeeding lines. Section **2** introduces the influence of charge in Einstein's field equations for a static spherical interior possessing two sources, i.e., initial anisotropic and newly added fluids. A well-known geometric transformation is applied on the formulated field equations in section **3**, resulting into two sets. Different constraints on both systems of equations are employed independently and find the corresponding solutions in sections **4** and **5**. Section **6** discusses the influence of the decoupling technique and charge on physical attributes of the resulting models. On a final note, we summarize all our results in section **7**.

2 Static Spherical Geometry and Einstein-Maxwell Framework

We present the field equations in this section that describe a static spherical spacetime influenced by an electromagnetic field. The spherical geometry $(t, r, \theta, \vartheta)$ is considered to split into two sectors, namely exterior and interior regions over the hypersurface Σ . In order to perform our analysis, the interior spacetime is given by the line element as

$$ds^2 = -e^{\xi_1} dt^2 + e^{\xi_2} dr^2 + r^2 d\Omega^2, \quad (1)$$

where $\xi_1 = \xi_1(r)$, $\xi_2 = \xi_2(r)$ and $d\Omega^2 = d\theta^2 + \sin^2 \theta d\vartheta^2$. The presence of Lagrangian corresponding to the additional source and electromagnetic field in the Einstein-Hilbert action produces the field equations given by

$$G_{\lambda\chi} = R_{\lambda\chi} - \frac{1}{2}Rg_{\lambda\chi} = 8\pi\bar{T}_{\lambda\chi}, \quad (2)$$

with

$$\bar{T}_{\lambda\chi} = T_{\lambda\chi} + E_{\lambda\chi} + \omega Z_{\lambda\chi}, \quad (3)$$

where the quantities are expressed as

- $G_{\lambda\chi}$ is the Einstein tensor that characterizes the geometry,
- $R_{\lambda\chi}$, R and $g_{\lambda\chi}$ indicate the Ricci tensor, Ricci scalar and the metric tensor, respectively,
- $T_{\lambda\chi}$ is the usual matter EMT,
- $E_{\lambda\chi}$ is the electromagnetic EMT,
- $Z_{\lambda\chi}$ is the additional matter source gravitationally associated with $T_{\lambda\chi}$.

Since our aim is to study the complexity of a self-gravitating system, we must assume anisotropy in the interior initially whose EMT is defined by

$$T_{\lambda\chi} = (P_t + \rho)W_\lambda W_\chi + P_t g_{\lambda\chi} - (P_t - P_r)X_\lambda X_\chi, \quad (4)$$

where P_r , P_t , ρ , W_χ and X_χ are the radial/tangential pressure elements, energy density, four-velocity and the four-vector, respectively. We consider

a co-moving frame of reference that gives rise to the following quantities in accordance with Eqs.(1) and (4) as

$$X^\chi = (0, e^{-\frac{\xi_2}{2}}, 0, 0), \quad W^\chi = (e^{-\frac{\xi_1}{2}}, 0, 0, 0),$$

fulfilling the relations

$$X^\chi W_\chi = 0, \quad X^\chi X_\chi = 1, \quad W^\chi W_\chi = -1.$$

The electromagnetic field characterized by the EMT is expressed as

$$E_{\lambda\chi} = -\frac{1}{4\pi} \left[\frac{1}{4} g_{\lambda\chi} F^{\zeta\beta} F_{\zeta\beta} - F_\chi^\zeta F_{\lambda\zeta} \right]. \quad (5)$$

Here, the Maxwell field tensor is represented by $F_{\zeta\beta} = \Psi_{\beta;\zeta} - \Psi_{\zeta;\beta}$ with the four-potential $\Psi_\zeta = \Psi(r)\delta_\zeta^0$. The Maxwell equations can concisely be written as follows

$$F_{;\beta}^{\zeta\beta} = 4\pi j^\zeta, \quad F_{[\zeta\beta;\nu]} = 0,$$

with $j^\zeta = \varpi W^\zeta$ and ϖ being the current and charge densities, respectively. The left side of the above equations yields in this framework as

$$\Psi'' + \frac{1}{2r} \{4 - r(\xi'_1 + \xi'_2)\} \Psi' = 4\pi\varpi e^{\frac{\xi_1}{2} + \xi_2},$$

where $' = \frac{\partial}{\partial r}$. Integrating the above equation, we have

$$\Psi' = \frac{q}{r^2} e^{\frac{\xi_1 + \xi_2}{2}},$$

with $q = \int_0^r \varpi e^{\frac{\xi_2}{2}} \bar{y}^2 d\bar{y}$ being the total charge in the interior. The non-vanishing components of the EMTs (4) and (5) are

$$\begin{aligned} T_{00} &= \rho e^{\xi_1}, & T_{11} &= P_r e^{\xi_2}, & T_{22} &= P_t r^2 = \frac{T_{33}}{\sin^2 \theta}, \\ E_{00} &= \frac{q^2 e^{\xi_1}}{8\pi r^4}, & E_{11} &= -\frac{q^2 e^{\xi_2}}{8\pi r^4}, & E_{22} &= \frac{q^2}{8\pi r^2} = \frac{E_{33}}{\sin^2 \theta}. \end{aligned}$$

The three independent field equations corresponding to a sphere (1) are obtained from Eq.(2) as

$$8\pi\rho + \frac{q^2}{r^4} - 8\pi\omega Z_0^0 = \frac{1}{r^2} - e^{-\xi_2} \left(\frac{1}{r^2} - \frac{\xi'_2}{r} \right), \quad (6)$$

$$8\pi P_r - \frac{q^2}{r^4} + 8\pi\omega Z_1^1 = e^{-\xi_2} \left(\frac{1}{r^2} + \frac{\xi_1'}{r} \right) - \frac{1}{r^2}, \quad (7)$$

$$8\pi P_t + \frac{q^2}{r^4} + 8\pi\omega Z_2^2 = \frac{e^{-\xi_2}}{4} \left[\xi_1'^2 - \xi_1' \xi_2' + 2\xi_1'' - \frac{2\xi_2'}{r} + \frac{2\xi_1}{r} \right]. \quad (8)$$

The conservation equation in this case can be obtained by taking the covariant divergence of the total fluid (seed, charge and additional), i.e., $\nabla^\lambda (T_{\lambda\chi} + E_{\lambda\chi} + \omega Z_{\lambda\chi}) = 0$ as

$$\begin{aligned} \frac{dP_r}{dr} + \frac{\xi_1'}{2}(\rho + P_r) + \frac{\omega\xi_1'}{2}(Z_1^1 - Z_0^0) + \frac{2}{r}(P_r - P_t) \\ + \omega \frac{dZ_1^1}{dr} + \frac{2\omega}{r}(Z_1^1 - Z_2^2) - \frac{qq'}{4\pi r^4} = 0. \end{aligned} \quad (9)$$

The above condition must hold for the system to be in a stable equilibrium, called the Tolman-Oppenheimer-Volkoff (TOV) equation. The mass function can be specified in terms of geometry as well as matter distribution. The geometric definition is given by

$$m(r) = \frac{r}{2} \left(1 - \frac{1}{e^{\xi_2}} + \frac{q^2}{r^2} \right). \quad (10)$$

On the other hand, the mass in relation with the energy density and charge can be obtained through Eqs.(6) and (10) as

$$\begin{aligned} m(r) &= 4\pi \int_0^r \rho \bar{y}^2 d\bar{y} + \int_0^r \frac{qq'}{\bar{y}} d\bar{y} + 4\pi\omega \int_0^r Z_0^0 \bar{y}^2 d\bar{y} \\ &= 4\pi \int_0^r \rho \bar{y}^2 d\bar{y} + \frac{1}{2} \int_0^r \frac{q^2}{\bar{y}^2} d\bar{y} + \frac{q^2}{2r} + 4\pi\omega \int_0^r Z_0^0 \bar{y}^2 d\bar{y}, \end{aligned} \quad (11)$$

where the first three terms correspond to the mass of charged fluid distribution and the last term defines the mass related to the new source. We use Eq.(7) to determine the value of ξ_1' in terms of the mass function (10) as

$$\xi_1' = \frac{2\{4\pi(P_r + \omega Z_1^1)r^4 + mr - q^2\}}{r(r^2 - 2mr + q^2)}. \quad (12)$$

Switching the above value into Eq.(9), we get

$$\frac{dP_r}{dr} + \left[\frac{4\pi(P_r + \omega Z_1^1)r^4 + mr - q^2}{r(r^2 - 2mr + q^2)} \right] \{ \rho + P_r + \omega(Z_1^1 - Z_0^0) \}$$

$$+ \frac{2}{r}(P_r - P_t) + \omega \frac{dZ_1^1}{dr} + \frac{2\omega}{r}(Z_1^1 - Z_2^2) - \frac{q q'}{4\pi r^4} = 0, \quad (13)$$

where $\Pi = P_t - P_r$ and $\Pi_Z = Z_2^2 - Z_1^1$ are the anisotropic factors corresponding to the seed and additional fluid sources, respectively.

3 Gravitational Decoupling

Since we include an additional source in the initial anisotropic fluid, the corresponding field equations now become difficult to solve due to the increment of unknowns, i.e., $(\xi_1, \xi_2, q, \rho, P_t, P_r, Z_0^0, Z_1^1, Z_2^2)$. Thus, we need to adopt certain approach or constraints and reduce the degrees of freedom to get an exact solution. On that note, we start off with a systematic technique (referred to the gravitational decoupling [26]) whose implementation on the field equations makes it possible to find their solution. The exciting feature of this strategy is that it transforms the temporal/radial metric potentials to a new frame of reference and make the set of equations easy to handle. For this, we consider the following metric as a solution to Eqs.(6)-(8) given by

$$ds^2 = -e^{\xi_3(r)} dt^2 + \frac{1}{\xi_4(r)} dr^2 + r^2 d\Omega^2. \quad (14)$$

In this context, the metric components linearly transform as

$$\xi_3 \rightarrow \xi_1 = \xi_3 + \omega f, \quad \xi_4 \rightarrow e^{-\xi_2} = \xi_4 + \omega t, \quad (15)$$

along with the temporal f and radial t deformation functions.

We choose the MGD scheme, thus only the g_{rr} component is deformed in the following, while keeping g_{tt} potential remains unchanged, i.e., $t \rightarrow \bar{t}$, $f \rightarrow 0$. Equation (15) now turns into

$$\xi_3 \rightarrow \xi_1 = \xi_3, \quad \xi_4 \rightarrow e^{-\xi_2} = \xi_4 + \omega \bar{t}, \quad (16)$$

where $\bar{t} = \bar{t}(r)$. It is important to note that the spherical symmetry remains preserved by these linear mappings. We implement the transformation (16) on Eqs.(6)-(8) and obtain two systems. The first set portraying the seed fluid source is acquired for $\omega = 0$ as

$$8\pi\rho + \frac{q^2}{r^4} = e^{-\xi_2} \left(\frac{\xi_2'}{r} - \frac{1}{r^2} \right) + \frac{1}{r^2}, \quad (17)$$

$$8\pi P_r - \frac{q^2}{r^4} = e^{-\xi_2} \left(\frac{1}{r^2} + \frac{\xi_1'}{r} \right) - \frac{1}{r^2}, \quad (18)$$

$$8\pi P_t + \frac{q^2}{r^4} = \frac{e^{-\xi_2}}{4} \left(\xi_1'^2 - \xi_2' \xi_1' + 2\xi_1'' - \frac{2\xi_2'}{r} + \frac{2\xi_1'}{r} \right). \quad (19)$$

Furthermore, the impact of the newly added source $Z_{\lambda\chi}$ is encoded by the following set and can be obtained for $\omega = 1$ as

$$8\pi Z_0^0 = \frac{1}{r} \left(\bar{t}' + \frac{\bar{t}}{r} \right), \quad (20)$$

$$8\pi Z_1^1 = \frac{\bar{t}}{r} \left(\xi_1' + \frac{1}{r} \right), \quad (21)$$

$$8\pi Z_2^2 = \frac{\bar{t}}{4} \left(2\xi_1'' + \xi_1'^2 + \frac{2\xi_1'}{r} \right) + \frac{\bar{t}'}{2} \left(\frac{\xi_1'}{2} + \frac{1}{r} \right). \quad (22)$$

Since we have used the MGD scheme, both matter sources must be conserved individually because the exchange of energy is not permitted in this case. The following two equations confirm the conservation of these sources as

$$\frac{dP_r}{dr} + \frac{\xi_1'}{2} (\rho + P_r) + \frac{2}{r} (P_r - P_t) - \frac{qq'}{4\pi r^4} = 0, \quad (23)$$

$$\frac{dZ_1^1}{dr} + \frac{\xi_1'}{2} (Z_1^1 - Z_0^0) + \frac{2}{r} (Z_1^1 - Z_2^2) = 0. \quad (24)$$

We observe that the system (17)-(19) possesses six unknown quantities $(\rho, P_r, P_t, q, \xi_1, \xi_2)$, therefore, we need to choose three of them freely to calculate the required analytical solution. Further, there are four unknowns $(\bar{t}, Z_0^0, Z_1^1, Z_2^2)$ in the second set (20)-(22). We shall adopt a constraint on the Z -sector to tackle with the second system. We detect the effective forms of the physical determinants as

$$\bar{\rho} = \rho - \omega Z_0^0, \quad (25)$$

$$\bar{P}_r = P_r + \omega Z_1^1, \quad (26)$$

$$\bar{P}_t = P_t + \omega Z_2^2, \quad (27)$$

with the total anisotropy given by

$$\bar{\Pi} = \bar{P}_t - \bar{P}_r = (P_t - P_r) + \omega (Z_2^2 - Z_1^1) = \Pi + \Pi_Z. \quad (28)$$

It must be mentioned that the presence of positive or negative anisotropy can significantly influence the stability of a compact star. The positive anisotropy (when radial pressure is less than the tangential component) can increase the stability of a compact star as it produces outward-directed pressure. This pressure provides a support against the gravitational attraction and prevents a star from collapse. On the other hand, the negative anisotropy (when radial pressure is greater than the tangential component) can lead to instability of the star as the pressure in the outward direction is not produced. Thus, such a star remains stable for a short period of time as compared to that possessing positive anisotropy. Further, the TOV equation (9) can be written as

$$\frac{d\bar{P}_r}{dr} + \frac{\xi'_1}{2}(\bar{\rho} + \bar{P}_r) + \frac{2}{r}(\bar{P}_r - \bar{P}_t) - \frac{qq'}{4\pi r^4} = 0. \quad (29)$$

which is a combination of different forces. The four terms on the left side of the above equation represent hydrostatic (f_h), gravitational (f_g), anisotropic (f_a) and electromagnetic (f_e) forces, respectively that must be satisfied to maintain hydrostatic equilibrium of a self-gravitating object. The concise notation of Eq.(29) is

$$f_h + f_a + f_w = 0, \quad (30)$$

where $f_w = f_g + f_e$.

4 Isotropization of Anisotropic Compact Fluid Sources

The anisotropy triggered in a self-gravitating system due to the original charged fluid source is entirely different from the anisotropic factor produced by the total configuration (seed and additional sources). In this section, we provide a brief study that how the anisotropic interior can be converted into the isotropic analog. In other words, we find the conditions under which the considered matter distribution becomes isotropic, i.e., $\bar{\Pi} = 0$. Following lines show such structural conversion is being controlled by the decoupling parameter. We observe that the vanishing decoupling parameter ($\omega = 0$) leads to the anisotropic system, while $\omega = 1$ corresponds to the isotropic framework. Since we are interested in discussing the second case, thus Eq.(28) yields

$$\Pi_Z = -\Pi \quad \Rightarrow \quad Z_2^2 - Z_1^1 = P_r - P_t. \quad (31)$$

The construction of minimally/extended decoupled isotropic interiors from being anisotropic have been done by taking the above condition into account [43, 47].

We now assume a specific metric ansatz to deal with the extra degrees of freedom in the system (17)-(19) defined by

$$\xi_1(r) = \ln \left\{ C_2^2 \left(1 + \frac{r^2}{C_1^2} \right) \right\}, \quad (32)$$

$$\xi_4(r) = e^{-\xi_2} = \frac{C_1^2 + r^2}{C_1^2 + 3r^2}, \quad (33)$$

whose substitution makes the matter triplet as

$$\rho = \frac{6r^4(C_1^2 + r^2) - (C_1^2 + 3r^2)^2 q^2}{8\pi r^4 (C_1^2 + 3r^2)^2}, \quad (34)$$

$$P_r = \frac{q^2}{8\pi r^4}, \quad (35)$$

$$P_t = \frac{3r^6 - (C_1^2 + 3r^2)^2 q^2}{8\pi r^4 (C_1^2 + 3r^2)^2}, \quad (36)$$

with C_1^2 and C_2^2 being unknown functions and the junction conditions are used in the following to make them known. It is important to stress that the metric ansatz (32) and (33) correspond only to the tangential pressure in the uncharged case while the radial component disappears [43]. However, they both appear in the current scenario due to the presence of an electromagnetic field. The same metric potentials have also been employed in the study of circular-like motion of different particles in their field of gravitation [48].

Junction conditions are a subject of great discussion of all time for astrophysicists which assist the study of multiple physical factors in a self-gravitating interior at the hypersurface, i.e., $\Sigma : r = \mathcal{R}$. The smooth matching requires an interior and exterior metrics representing the corresponding spacetime regions of the considered geometry. Since we have already defined the interior metric in Eq.(1), a suitable exterior geometry in this regard is the Reissner-Nordström line element (a solution to the charged vacuum spacetime) given by

$$ds^2 = - \left(1 - \frac{2\mathcal{M}}{r} + \frac{\mathcal{Q}^2}{r^2} \right) dt^2 + \frac{1}{\left(1 - \frac{2\mathcal{M}}{r} + \frac{\mathcal{Q}^2}{r^2} \right)} dr^2 + r^2 d\Omega^2, \quad (37)$$

with \mathcal{Q} is the total charge and \mathcal{M} symbolizes the corresponding mass. We now obtain the two constants (C_1^2 , C_2^2) by equating the temporal/radial metrics components of the metrics (1) and (37) as

$$C_1^2 = \frac{\mathcal{R}^2(2\mathcal{R}^2 + 3\mathcal{Q}^2 - 6\mathcal{M}\mathcal{R})}{2\mathcal{M}\mathcal{R} - \mathcal{Q}^2}, \quad (38)$$

$$C_2^2 = \frac{2\mathcal{R}^2 + 3\mathcal{Q}^2 - 6\mathcal{M}\mathcal{R}}{2\mathcal{R}^2}. \quad (39)$$

The radius ($\mathcal{R} = 9.1 \pm 0.4 \text{ km}$) and mass ($\mathcal{M} = 1.58 \pm 0.06$ times the sun's mass) of a specific compact model $4U\ 1820 - 30$ is considered to plot the resulting solutions in the following sections [49]. Further, we observe that one extra unknown is still present in the system (34)-(36), thus $q^2(r) = \xi_5 r^6$ is assumed with ξ_5 as a constant [35]. Joining this with the restriction (31) and field equations, a differential equation is obtained as

$$r(C_1^2 + r^2) [2r^3(C_1^2 + r^2)(2\xi_5 C_1^4 + 12\xi_5 C_1^2 r^2 + 18\xi_5 r^4 - 3) - (C_1^2 + 2r^2) \times (C_1^2 + 3r^2)^2 \bar{t}'(r)] + 2(C_1^4 + 2C_1^2 r^2 + 2r^4)(C_1^2 + 3r^2)^2 \bar{t}(r) = 0, \quad (40)$$

whose exact solution provides $\bar{t}(r)$ as

$$\bar{t}(r) = \frac{r^2(C_1^2 + r^2)}{C_1^2 + 2r^2} \left\{ D_1 + 2\xi_5 r^2 + \frac{2\xi_5 C_1^2}{3} + \frac{1}{C_1^2 + 3r^2} \right\}, \quad (41)$$

with D_1 as an integration constant whose dimension is $\frac{1}{\ell^2}$. It is well-known that the radial pressure vanishes at the spherical junction, i.e., $\bar{P}_r(\mathcal{R}) = 0$. Hence, Eq.(26) along with (35) and (41) provides D_1 as

$$D_1 = -2\xi_5 \mathcal{R}^2 - \frac{2\xi_5 C_1^2}{3} - \frac{1}{C_1^2 + 3\mathcal{R}^2} - \frac{\xi_5 \mathcal{R}^2 (C_1^2 + 2\mathcal{R}^2)}{\omega(C_1^2 + 3\mathcal{R}^2)}. \quad (42)$$

Equation (41) now takes the form

$$\bar{t}(r) = \frac{r^2(C_1^2 + r^2)}{C_1^2 + 2r^2} \left\{ 2\xi_5 (r^2 - \mathcal{R}^2) - \frac{3(r^2 - \mathcal{R}^2)}{(C_1^2 + 3r^2)(C_1^2 + 3\mathcal{R}^2)} - \frac{\xi_5 \mathcal{R}^2 (C_1^2 + 2\mathcal{R}^2)}{\omega(C_1^2 + 3\mathcal{R}^2)} \right\}, \quad (43)$$

and the deformed g_{rr} metric component becomes

$$e^{\xi_2} = \xi_4^{-1} = [r^2(C_1^2 + r^2) \{ -\xi_5(C_1^2 + 3r^2)(C_1^2(\mathcal{R}^2(2\omega + 1) - 2r^2\omega) + 2\mathcal{R}^2$$

$$\begin{aligned} & \times (\mathcal{R}^2(3\omega + 1) - 3r^2\omega) - 3\omega(r^2 - \mathcal{R}^2)\} + (C_1^2 + r^2)(C_1^2 + 2r^2) \\ & \times (C_1^2 + 3\mathcal{R}^2)]^{-1} [(C_1^2 + 2r^2)(C_1^2 + 3r^2)(C_1^2 + 3\mathcal{R}^2)]. \end{aligned} \quad (44)$$

Finally, the decoupled solution to the system (6)-(8) is expressed by the line element as follows

$$ds^2 = -C_2^2 \left(1 + \frac{r^2}{C_1^2}\right) dt^2 + \frac{C_1^2 + 3r^2}{C_1^2 + r^2 + \omega \bar{t}(r)(C_1^2 + 3r^2)} dr^2 + r^2 d\Omega^2, \quad (45)$$

along with the matter triplet given by

$$\begin{aligned} \bar{\rho} = & \frac{C_1^2(6 - 6\xi_5 r^4) - C_1^4 \xi_5 r^2 - 9\xi_5 r^6 + 6r^2}{8\pi(C_1^2 + 3r^2)^2} - [8\pi r^2 (C_1^2 + r^2)^2 \{C_1^4 (\xi_5 r^2 \\ & \times (2r^2\omega - \mathcal{R}^2(2\omega + 1)) + 1) + C_1^2(2r^2 + \xi_5 r^2(6r^4\omega - 3r^2\mathcal{R}^2 - 2\mathcal{R}^4 \\ & \times (3\omega + 1)) + 3\mathcal{R}^2) + 3r^2(2\xi_5 r^2 \mathcal{R}^2(3r^2\omega - \mathcal{R}^2(3\omega + 1)) - \omega r^2 + \mathcal{R}^2 \\ & \times (\omega + 2))\}^2]^{-1} [\omega(C_1^2 + 3\mathcal{R}^2) \{C_1^{10} (\xi_5 r^2 (\mathcal{R}^2(2\omega + 1) - 6r^2\omega) + 1) \\ & + C_1^8 (3(4r^2 + \mathcal{R}^2) + \xi_5 r^2 (-50r^4\omega + r^2\mathcal{R}^2(7 - 4\omega) + 2\mathcal{R}^4(3\omega + 1))) \\ & + C_1^6 r^2 (r^2(9\omega + 39) + \xi_5 r^2 (r^2\mathcal{R}^2(17 - 116\omega) + 14\mathcal{R}^4(3\omega + 1) - 150r^4\omega \\ & - 3\mathcal{R}^2(\omega - 12)) + C_1^4 r^4 (r^2(30\omega + 44) + \xi_5 r^2 (3r^2\mathcal{R}^2(7 - 136\omega) - 198r^4\omega \\ & + 34\mathcal{R}^4(3\omega + 1)) + 3\mathcal{R}^2(2\omega + 39)) + 3C_1^2 r^6 (r^2(9\omega + 4) + 2\xi_5 r^2 (-18r^4\omega \\ & + 3r^2\mathcal{R}^2(1 - 31\omega) + 7\mathcal{R}^4(3\omega + 1)) + \mathcal{R}^2(13\omega + 44)) + 18r^8 (2\xi_5 r^2 \mathcal{R}^2 (\mathcal{R}^2 \\ & \times (3\omega + 1) - 9r^2\omega) + r^2\omega + \mathcal{R}^2(\omega + 2))\}], \end{aligned} \quad (46)$$

$$\begin{aligned} \bar{P}_r = & \frac{1}{8\pi} \left[\xi_5 r^2 + \omega \left(\frac{C_1^2 + 3r^2}{C_1^2 + 2r^2} \right) \left\{ 2\xi_5 (r^2 - \mathcal{R}^2) - \frac{3(r^2 - \mathcal{R}^2)}{(C_1^2 + 3r^2)(C_1^2 + 3\mathcal{R}^2)} \right. \right. \\ & \left. \left. - \frac{\xi_5 \mathcal{R}^2 (C_1^2 + 2\mathcal{R}^2)}{\omega (C_1^2 + 3\mathcal{R}^2)} \right\} \right], \end{aligned} \quad (47)$$

$$\begin{aligned} \bar{P}_t = & \frac{r^2(3 - C_1^4 \xi_5 - 6C_1^2 \xi_5 r^2 - 9\xi_5 r^4)}{8\pi(C_1^2 + 3r^2)^2} + \frac{\omega r^2(2C_1^2 + r^2)}{8\pi(C_1^2 + r^2)(C_1^2 + 2r^2)} \\ & \times \left\{ 2\xi_5 (r^2 - \mathcal{R}^2) - \frac{3(r^2 - \mathcal{R}^2)}{(C_1^2 + 3r^2)(C_1^2 + 3\mathcal{R}^2)} - \frac{\xi_5 \mathcal{R}^2 (C_1^2 + 2\mathcal{R}^2)}{\omega (C_1^2 + 3\mathcal{R}^2)} \right\} - \frac{\omega}{8\pi} \\ & \times [(C_1^2 + r^2)^3 (\xi_5 r^2 (C_1^2 + 3r^2) (C_1^2 (2r^2\omega - \mathcal{R}^2(2\omega + 1)) + 2\mathcal{R}^2 (3r^2\omega \\ & - \mathcal{R}^2(3\omega + 1))) + C_1^2 (C_1^2 + 2r^2 + 3\mathcal{R}^2) + 3r^2 (\mathcal{R}^2(\omega + 2) - r^2\omega))^2]^{-1} \\ & \times [(C_1^2 + 2r^2)(C_1^2 + 3\mathcal{R}^2) \{ -2C_1^4 r^2 (4r^2(3\omega + 1) - 3\mathcal{R}^2(\omega - 4)) - C_1^6 \end{aligned}$$

$$\begin{aligned}
& \times (r^2(6\omega + 8) - 3\mathcal{R}^2(\omega - 2)) - 3C_1^2 r^4 (10r^2\omega + \mathcal{R}^2(\omega + 8)) + \xi_5 (C_1^2 \\
& + 3r^2)^2 (C_1^6 (- (\mathcal{R}^2(2\omega + 1) - 4r^2\omega)) + 2C_1^4 (5r^4\omega + r^2\mathcal{R}^2(4\omega - 1)\mathcal{R}^4 \\
& - \times (3\omega + 1)) + 2C_1^2 r^2 (4r^4\omega + r^2\mathcal{R}^2(13\omega - 1) - 2\mathcal{R}^4(3\omega + 1)) + 4r^4\mathcal{R}^2 \\
& \times (6r^2\omega - \mathcal{R}^2(3\omega + 1))) - 2C_1^8 - 18r^8\omega \}. \tag{48}
\end{aligned}$$

The anisotropy in the interior of the above developed model is

$$\bar{\Pi} = \frac{r^2(3 - 2\xi_5 C_1^4 - 12\xi_5 C_1^2 r^2 - 18\xi_5 r^4)}{8\pi(C_1^2 + 3r^2)^2} (1 - \omega). \tag{49}$$

It becomes clear from the above equation that the anisotropy fades away for $\omega = 1$, hence, the total matter distribution turns into the isotropic interior for this particular value. We can now say that Eqs.(46)-(49) are the analytical solution of the Einstein-Maxwell field equations for $\omega \in [0, 1]$. In other words, the variation in this parameter produces the isotropic configuration from being anisotropic and vice versa.

5 Complexity Analysis and Compact Fluid Sources

Herrera [38] defined complexity for the first time in such a way that could be suitable for all scientific fields. According to this definition, a uniform/homogenous system is always complexity-free, implying that the density inhomogeneity and anisotropy in the pressure make the structure complex. Multiple structure scalars, in this context, were obtained corresponding to a static spherical interior through the orthogonal decomposition of the curvature tensor. Both the above-mentioned factors were found in one of the scalars, i.e., Y_{TF} and thus entitled the complexity factor. This work was also extended for a non-static scenario where some evolutionary patterns have been discussed [39]. For the charged scenario, the factor Y_{TF} becomes

$$Y_{TF}(r) = 8\pi\Pi + \frac{4q^2}{r^4} - \frac{4\pi}{r^3} \int_0^r \bar{y}^3 \rho'(\bar{y}) d\bar{y} - \frac{3}{r^3} \int_0^r \frac{qq'}{\bar{y}} d\bar{y}. \tag{50}$$

Since the current setup (6)-(8) involves two matter sources, thus the corresponding extension of the complexity factor is given by

$$\bar{Y}_{TF}(r) = 8\pi\bar{\Pi} + \frac{4q^2}{r^4} - \frac{4\pi}{r^3} \int_0^r \bar{y}^3 \bar{\rho}'(\bar{y}) d\bar{y} - \frac{3}{r^3} \int_0^r \frac{q\bar{q}'}{\bar{y}} d\bar{y}$$

$$\begin{aligned}
&= 8\pi\Pi + \frac{4q^2}{r^4} - \frac{4\pi}{r^3} \int_0^r \bar{y}^3 \rho'(\bar{y}) d\bar{y} - \frac{3}{r^3} \int_0^r \frac{qq'}{\bar{y}} d\bar{y} \\
&+ 8\pi\omega\Pi_Z + \frac{4\pi\omega}{r^3} \int_0^r \bar{y}^3 Z_0^{0'}(\bar{y}) d\bar{y}, \tag{51}
\end{aligned}$$

which can also be written as

$$\bar{Y}_{TF} = Y_{TF} + Y_{TF}^Z. \tag{52}$$

Here, Y_{TF} and Y_{TF}^Z are the complexity factors for the sources (17)-(19) and (20)-(22), respectively. Since we develop the model (46)-(49) by taking $\bar{\Pi} = 0$ into account, therefore, Eq.(51) leads to

$$\bar{Y}_{TF} = \frac{4q^2}{r^4} - \frac{4\pi}{r^3} \int_0^r \bar{y}^3 \bar{\rho}'(\bar{y}) d\bar{y} - \frac{3}{r^3} \int_0^r \frac{qq'}{\bar{y}} d\bar{y}. \tag{53}$$

After substituting the derivative of the effective energy density (46) in the above equation, we get

$$\begin{aligned}
\bar{Y}_{TF} &= \frac{11\xi_5 r^2}{5} + \frac{r^2}{5(C_1^4 + 5C_1^2 r^2 + 6r^4)^2 (C_1^2 + 3\mathcal{R}^2)} [C_1^{10}(10\xi_5\omega + \xi_5) + 2\xi_5 \\
&\times C_1^8(5(8\omega + 1)r^2 + 4(5\omega + 1)\mathcal{R}^2) + C_1^6(\xi_5(230\omega + 37)r^4 + 60\xi_5 r^2 \mathcal{R}^2 \\
&(5\omega + 1) + 5(2\xi_5(3\omega + 1)\mathcal{R}^4 + 6 - 3\omega)) + 6C_1^4(10r^6(5\xi_5\omega + \xi_5) + 26\xi_5 \\
&\times (5\omega + 1)r^4 \mathcal{R}^2 + 5r^2(2\xi_5(3\omega + 1)\mathcal{R}^4 + 4 - \omega) + 5(3 - 2\omega)\mathcal{R}^2) + 3C_1^2 \\
&\times r^2(12r^6(5\xi_5\omega + \xi_5) + 60\xi_5(5\omega + 1)r^4 \mathcal{R}^2 - 60(\omega - 2)\mathcal{R}^2 + 5r^2(\omega + 6 \\
&\times \xi_5(3\omega + 1)\mathcal{R}^4 + 8)) + 18r^4 \mathcal{R}^2(6r^4(5\xi_5\omega + \xi_5) - 5(\omega - 4))]. \tag{54}
\end{aligned}$$

5.1 Complexity-free additional Matter Source

Here we consider the additional fluid source to be the complexity-free (i.e., $Y_{TF}^Z = 0$) as an extra constraint so that the system (20)-(22) can be solved uniquely. After engaging this with Eq.(52), we observe that $\bar{Y}_{TF} = Y_{TF}$ or, equivalently

$$\Pi_Z = -\frac{1}{2r^3} \int_0^r \bar{y}^3 Z_0^{0'}(\bar{y}) d\bar{y}. \tag{55}$$

The integral on the right side of Eq.(55) can be manipulated by using (20) as

$$\int_0^r \bar{y}^3 Z_0^{0'}(\bar{y}) d\bar{y} = r^2 \bar{t}'(r) - 2r \bar{t}(r), \tag{56}$$

whose substitution along with Eqs.(21) and (22) in (55) results in the first-order differential equation as follows

$$\bar{t}'(r) \left(\frac{\xi_1'}{4} + \frac{1}{r} \right) + \bar{t}(r) \left(\frac{\xi_1''}{2} - \frac{2}{r^2} + \frac{\xi_1'^2}{4} - \frac{\xi_1'}{2r} \right) = 0. \quad (57)$$

The above equation contains the metric coefficient, thus the solution for $\bar{t}(r)$ is possible only if we consider a particular metric ansatz. In order to continue our study, we take Tolman IV metric components given in the following

$$\xi_1(r) = \ln \left\{ C_2^2 \left(1 + \frac{r^2}{C_1^2} \right) \right\}, \quad (58)$$

$$\xi_4(r) = e^{-\xi_2(r)} = \frac{(C_1^2 + r^2)(C_3^2 - r^2)}{C_3^2(C_1^2 + 2r^2)}, \quad (59)$$

characterizing the isotropic interior through the following density and pressure as

$$\rho = \frac{C_1^4(3 - \xi_5 r^2 C_3^2) + C_1^2(7r^2 - 4\xi_5 r^4 C_3^2 + 3C_3^2) - 4\xi_5 r^6 C_3^2 + 6r^4 + 2r^2 C_3^2}{8\pi C_3^2(C_1^2 + 2r^2)^2}, \quad (60)$$

$$P = \frac{\xi_5 C_1^2 r^2 C_3^2 - C_1^2 + 2\xi_5 r^4 C_3^2 - 3r^2 + C_3^2}{8\pi C_1^2 C_3^2 + 16\pi r^2 C_3^2}. \quad (61)$$

The values of C_1^2 and C_2^2 are already obtained in Eqs.(38) and (39), however, the newly introduced constant C_3^2 becomes

$$C_3^2 = \frac{2\mathcal{R}^3(\mathcal{Q}^2 - 2\mathcal{M}\mathcal{R} + \mathcal{R}^2)}{2\mathcal{M}\mathcal{Q} - 4\mathcal{M}^2\mathcal{R} + \mathcal{Q}\mathcal{R} + 2\mathcal{M}\mathcal{R}^2}. \quad (62)$$

Inserting Eq.(58) in (57) and simplifying, we obtain

$$r(2C_1^4 + 5C_1^2 r^2 + 3r^4)\bar{t}'(r) - 2(2C_1^4 + 4C_1^2 r^2 + 3r^4)\bar{t}(r) = 0, \quad (63)$$

whose solution is

$$\bar{t}(r) = \frac{D_2 r^2 (C_1^2 + r^2)}{2C_1^2 + 3r^2}, \quad (64)$$

along with a constant D_2 having dimension of $\frac{1}{l^2}$. We again use $\bar{P}_r(\mathcal{R}) = P_r(\mathcal{R}) + \omega Z_1^1(\mathcal{R}) = 0$ to calculate D_2 and simplification gives

$$D_2 = \frac{(C_1^2 - C_3^2 + 3\mathcal{R}^2 - \xi_5 \mathcal{R}^2 C_1^2 C_3^2 - 2\xi_5 \mathcal{R}^4 C_3^2)(2C_1^2 + 3\mathcal{R}^2)}{\omega C_3^2(C_1^2 + 2\mathcal{R}^2)(C_1^2 + 3\mathcal{R}^2)}. \quad (65)$$

Consequently, the deformed expression of g_{rr} component becomes

$$e^{\xi_2} = \xi_4^{-1} = \frac{C_3^2(C_1^2 + 2r^2)(2C_1^2 + 3r^2)}{(C_1^2 + r^2)\{C_3^2(r^2\omega D_2(C_1^2 + 2r^2) + 2C_1^2 + 3r^2) - r^2(2C_1^2 + 3r^2)\}}. \quad (66)$$

Since the constraint (55) is based only on the additional matter source that does not have the influence of charge, the deformation function (64) is identical with the uncharged scenario [43]. Therefore, we do not need to physically interpret the corresponding model as this has already been done. Moreover, the factor \bar{Y}_{TF} (expressed in Eq.(51)) now becomes

$$\bar{Y}_{TF} = Y_{TF} = \frac{r^2(C_1^2 + 2C_3^2)}{C_3^2(C_1^2 + 2r^2)^2} + \frac{2\xi_5 r^2}{5}. \quad (67)$$

The above factor does not contain the decoupling parameter, thus we adopt the deformed g_{rr} metric component (66) to obtain the constant C_3^2 so that the variation of \bar{Y}_{TF} with respect to ω can be shown. We get this constant as

$$C_3^2 = 2\mathcal{R}^4(6M\mathcal{R} - 3Q^2 - 4\mathcal{R}^2)[2D_2\mathcal{R}^4\omega(2M\mathcal{R} - Q^2 - 2\mathcal{R}^2) + 4M\mathcal{R}^2(3M - 2\mathcal{R}) + Q^2(3Q^2 - 12M\mathcal{R} + 4\mathcal{R}^2)]^{-1}. \quad (68)$$

5.2 Complexity-free Total Matter Source

In this subsection, we try another constraint on the newly added source to make the Einstein-Maxwell field equations solvable so that a physically relevant compact interior can be modeled. We assume that the seed and additional sources may possess complexity individually, i.e., $Y_{TF} \neq 0$ and $Y_{TF}^Z \neq 0$, however, the system is no more complex once both sources merged, or equivalently, $\bar{Y}_{TF} = 0$. This assumption makes the scalar (52) in terms of Tolman IV ansatz as

$$\begin{aligned} & r(C_1^2 + r^2)[5C_3^2(C_1^2 + 2r^2)^2(2C_1^2 + 3r^2)\bar{t}'(r) + 2r^3(C_1^2 + r^2) \\ & \{2C_3^2C_1^4\xi_5 + 2C_3^2(4\xi_5r^4 + 5) + C_1^2(8C_3^2\xi_5r^2 + 5)\}] \\ & - 10C_3^2(C_1^2 + 2r^2)^2(4C_1^2r^2 + 2C_1^4 + 3r^4)\bar{t}(r) = 0, \end{aligned} \quad (69)$$

providing the function $\bar{t}(r)$ as follows

$$\bar{t}(r) = \frac{r^2(C_1^2 + r^2)}{5(2C_1^2 + 3r^2)} \left\{ 5 \left(\frac{1}{C_1^2 + 2r^2} + D_3 \right) - C_1^2 \xi_5 + \frac{5C_1^2}{C_3^2(2C_1^2 + 4r^2)} - 2\xi_5 r^2 \right\}, \quad (70)$$

where an arbitrary constant D_3 has a dimension $\frac{1}{l^2}$. Using Eq.(26) at the spherical junction, we get the value D_3 as

$$D_3 = \frac{1}{5C_3^2(C_1^2 + 2\mathcal{R}^2)} \left[\xi_5 C_3^2 (C_1^2 + 2\mathcal{R}^2)^2 - 5C_3^2 - \frac{5C_1^2}{2} + \frac{5\{C_1^2 - C_3^2 + 3\mathcal{R}^2 - \xi_5 \mathcal{R}^2 C_3^2 (C_1^2 + 2\mathcal{R}^2)\} (2C_1^2 + 3\mathcal{R}^2)}{\omega(C_1^2 + 3\mathcal{R}^2)} \right]. \quad (71)$$

Putting this back into Eq.(70), we obtain

$$\begin{aligned} \bar{t}(r) = & \frac{r^2(C_1^2 + r^2)}{10C_3^2(2C_1^2 + 3r^2)(C_1^2 + 2\mathcal{R}^2)} \left[(C_1^2 + 2\mathcal{R}^2) \left\{ \frac{5C_1^2}{C_1^2 + 2r^2} - 2C_3^2 \xi_5 \right. \right. \\ & \times (C_1^2 + 2r^2) \left. \left. \right\} + \frac{10C_3^2(C_1^2 + 2\mathcal{R}^2)}{C_1^2 + 2r^2} + 2C_3^2 \xi_5 (C_1^2 + 2\mathcal{R}^2)^2 - 10C_3^2 \right. \\ & \left. - 5C_1^2 + \frac{10(2C_1^2 + 3\mathcal{R}^2)(C_3^2 \xi_5 \mathcal{R}^2 (- (C_1^2 + 2\mathcal{R}^2)) + C_1^2 - C_3^2 + 3\mathcal{R}^2)}{\omega(C_1^2 + 3\mathcal{R}^2)} \right]. \end{aligned} \quad (72)$$

The corresponding modified form of g_{rr} metric potential can be expressed through the transformation (16) as

$$\begin{aligned} e^{\xi_2} = \xi_4^{-1} = & \frac{10C_3^2(C_1^2 + 2r^2)(2C_1^2 + 3r^2)(5C_1^2 \mathcal{R}^2 + C_1^4 + 6\mathcal{R}^4)}{r^2 + C_1^2} \\ & \times [10(2C_1^2 + 3r^2)(C_3^2 - r^2)(5C_1^2 \mathcal{R}^2 + C_1^4 + 6\mathcal{R}^4) - 2r^2 \{5C_3^2(C_1^2 \\ & \times (2r^2(\omega + 2) + \mathcal{R}^2(3 - 2\omega)) + 2C_1^4 + 6\mathcal{R}^2(r^2(\omega + 1) - \mathcal{R}^2\omega)) \\ & + 5(C_1^2 + 3\mathcal{R}^2)(C_1^2(r^2(\omega - 4) - \mathcal{R}^2(\omega + 3)) - 2C_1^4 - 6r^2 \mathcal{R}^2) \\ & + C_3^2 \xi_5 (C_1^2 + 2r^2)(C_1^2 + 2\mathcal{R}^2)(2C_1^2(r^2\omega + \mathcal{R}^2(5 - \omega)) + 6r^2 \mathcal{R}^2\omega \\ & + \mathcal{R}^4(15 - 6\omega))\}]^{-1}. \end{aligned} \quad (73)$$

Hence, the corresponding matter determinants take the final form as

$$\bar{\rho} = \frac{1}{40\pi C_3^2(7C_1^2 r^2 + 2C_1^4 + 6r^4)^2 (5C_1^2 \mathcal{R}^2 + C_1^4 + 6\mathcal{R}^4)} \left[4C_3^2 C_1^{12} \xi_5 \{(\omega - 1)\right.$$

$$\begin{aligned}
& \times 5r^2 + 3\mathcal{R}^2(5 - \omega)\} + 36C_3^2r^6\mathcal{R}^2\{2\xi_5r^2\mathcal{R}^2(5r^2(2\omega - 3) + 3\mathcal{R}^2(5 - 2\omega)) \\
& + 5(3r^2(\omega + 1) + \mathcal{R}^2(3 - \omega))\} + 2C_1^{10}\{C_3^2(\xi_5(7r^4(9\omega - 10) + (13\omega + 135) \\
& \times r^2\mathcal{R}^2 + 15\mathcal{R}^4(7 - 2\omega)) + 60) + 5(\omega - 1)(5r^2 - 3\mathcal{R}^2)\} + 6C_1^2r^4\{C_3^2(2\xi_5 \\
& \times r^2\mathcal{R}^2(25r^4(2\omega - 3) + r^2\mathcal{R}^2(122\omega - 105) + 44\mathcal{R}^4(5 - 2\omega)) + 5((\omega + 2) \\
& \times 6r^4 + r^2\mathcal{R}^2(39\omega + 59) + 3\mathcal{R}^4(17 - 5\omega))) + 15r^2\mathcal{R}^2(\omega - 1)(3r^2 - \mathcal{R}^2)\} \\
& + C_1^8\{C_3^2(10(r^2(10\omega + 59) + 3\mathcal{R}^2(13 - 2\omega)) + \xi_5(r^6(294\omega - 365) + 10\mathcal{R}^2 \\
& \times r^4(46\omega + 15) + 25r^2\mathcal{R}^4(47 - 10\omega) + 36\mathcal{R}^6(5 - 2\omega))) + 5(\omega - 1)(35r^4 \\
& + 13r^2\mathcal{R}^2 - 18\mathcal{R}^4)\} + C_1^6\{C_3^2(5(36\mathcal{R}^4(2 - \omega) + r^2\mathcal{R}^2(26\omega + 331) + r^4 \\
& \times (70\omega + 221)) + \xi_5r^2(4r^6(76\omega - 105) + r^4\mathcal{R}^2(1294\omega - 945) + r^2\mathcal{R}^4(2135 \\
& - 94\omega) + 222\mathcal{R}^6(5 - 2\omega))) + 5r^2(\omega - 1)(41r^4 + 90r^2\mathcal{R}^2 - 51\mathcal{R}^4)\} + C_1^4r^2 \\
& \times \{2C_3^2(5(r^4(41\omega + 97) + 15r^2\mathcal{R}^2(6\omega + 17) + 3\mathcal{R}^4(44 - 17\omega)) + \xi_5r^2(30r^6 \\
& \times (2\omega - 3) + 2r^4\mathcal{R}^2(362\omega - 435) + r^2\mathcal{R}^4(442\omega + 445) + 255\mathcal{R}^6(5 - 2\omega))) \\
& + 45r^2(\omega - 1)(2r^4 + 13r^2\mathcal{R}^2 - 5\mathcal{R}^4)\} \Big], \tag{74}
\end{aligned}$$

$$\begin{aligned}
\bar{P}_r = & \frac{1}{80\pi C_3^2(2C_1^2 + 3r^2)(C_1^2 + 2\mathcal{R}^2)} \left[\left(10C_3^2\xi_5r^2 - \frac{10(C_1^2 - C_3^2 + 3r^2)}{C_1^2 + 2r^2} \right) \right. \\
& \times (2C_1^2 + 3r^2)(C_1^2 + 2\mathcal{R}^2) + \omega(C_1^2 + 3r^2) \left\{ \frac{10C_3^2(C_1^2 + 2\mathcal{R}^2)}{C_1^2 + 2r^2} - 5C_1^2 + 2\xi_5 \right. \\
& \times C_3^2(C_1^2 + 2\mathcal{R}^2)^2 - 10C_3^2 + (C_1^2 + 2\mathcal{R}^2) \left(\frac{5C_1^2}{C_1^2 + 2r^2} - 2C_3^2\xi_5(C_1^2 + 2r^2) \right) \\
& \left. \left. + \frac{10(2C_1^2 + 3\mathcal{R}^2)(C_3^2\xi_5\mathcal{R}^2(- (C_1^2 + 2\mathcal{R}^2)) + C_1^2 - C_3^2 + 3\mathcal{R}^2)}{\omega(C_1^2 + 3\mathcal{R}^2)} \right\} \right], \tag{75}
\end{aligned}$$

$$\begin{aligned}
\bar{P}_t = & \frac{-1}{40\pi C_3^2(C_1^2 + 2r^2)(2C_1^2 + 3r^2)^2(5C_1^2\mathcal{R}^2 + C_1^4 + 6\mathcal{R}^4)} \left[4C_3^2C_1^{10}\{5\xi_5r^2 \right. \\
& + \xi_5(2r^2\omega - \mathcal{R}^2(\omega - 5))\} + 18C_3^2r^4\mathcal{R}^2\{2\xi_5r^2\mathcal{R}^2(10r^2\omega + \mathcal{R}^2(15 - 6\omega)) \\
& + 5(6\xi_5r^4\mathcal{R}^2 + 3r^2(\omega + 1) - \mathcal{R}^2(\omega + 3))\} + 2C_1^8\{C_3^2(50\xi_5r^2(r^2 + \mathcal{R}^2) \\
& + \xi_5(25r^4\omega + 2r^2\mathcal{R}^2(3\omega + 35) + 5\mathcal{R}^4(7 - 2\omega))) + 5(\omega - 1)(2r^2 - \mathcal{R}^2)\} \\
& + 3C_1^2r^2\{2C_3^2(\xi_5r^2\mathcal{R}^2(50r^4\omega + r^2\mathcal{R}^2(68\omega + 105) + 29\mathcal{R}^4(5 - 2\omega)) + 5 \\
& \times (15\xi_5r^6\mathcal{R}^2 + 3r^4(11\xi_5\mathcal{R}^4 + \omega + 2) + r^2\mathcal{R}^2(12\omega + 7) - 6\mathcal{R}^4(\omega + 2))) \\
& \left. + 15r^2\mathcal{R}^2(\omega - 1)(3r^2 - \mathcal{R}^2)\} + C_1^6\{C_3^2(5(33\xi_5r^6 + 100\xi_5r^4\mathcal{R}^2 + 8r^2(2
\end{aligned}$$

$$\begin{aligned}
& + 3\xi_5\mathcal{R}^4 + \omega) - 2\mathcal{R}^2(2\omega + 7)) + 2\xi_5(49r^6\omega + r^4\mathcal{R}^2(96\omega + 145) + r^2\mathcal{R}^4 \\
& \times (245 - 46\omega) + 6\mathcal{R}^6(5 - 2\omega))) + 5(\omega - 1)(13r^4 + 6r^2\mathcal{R}^2 - 6\mathcal{R}^4)\} + C_1^4 \\
& \times \{C_3^2(\xi_5r^2(60r^6\omega + 2r^4\mathcal{R}^2(227\omega + 90) + 5r^2\mathcal{R}^4(2\omega + 203) + (5 - 2\omega)84 \\
& \times \mathcal{R}^6) + 5(18\xi_5r^8 + 165\xi_5r^6\mathcal{R}^2 + r^4(120\xi_5\mathcal{R}^4 + 26\omega + 49) + 6r^2\mathcal{R}^2 \\
& \times (2\omega - 3) - 12\mathcal{R}^4(\omega + 2))) + 45r^2(\omega - 1)(r^4 + 4r^2\mathcal{R}^2 - 2\mathcal{R}^4)\}\}. \quad (76)
\end{aligned}$$

Further, Eqs.(75) and (76) can be used to obtain the corresponding pressure anisotropy.

6 Graphical Description of the Newly Obtained Models

The mass function corresponding to the charged spherical geometry is defined in Eq.(11). We put the effective energy densities (46) and (74) to observe how this factor behaves against r for our developed models. This function also helps to define the compactness and redshift of a self-gravitating system. The former parameter (symbolizes by $\tau(r)$) reveals the tightness of particles that how they arrange in a specific style. In other words, we can define it as the ratio of mass and radius of a compact body, thus an increasing function of r outwards. Several researchers have been tried to find its lower and upper bounds in a physically acceptable interior and the maximum value was found to be $\frac{4}{9}$ at the boundary [50]. Another parameter is known as the redshift which expresses the change in the wavelength of electromagnetic radiations ejecting from a massive object influenced by the strong gravitational field that nearby system produces. The mathematical notation is given by

$$z(r) = \frac{1 - \sqrt{1 - 2\tau(r)}}{\sqrt{1 - 2\tau(r)}}, \quad (77)$$

whose upper bound has been suggested in the literature as 2 and 5.211 for the case of perfect [50] and anisotropic [51] matter sources, respectively.

A subject of scientific debate for astrophysicists is to check the existence of an ordinary fluid in a compact interior. Multiple constraints, in this regard, gained much significance because they are used to check the physical viability of the models. These constraints are referred as the energy conditions, and

their satisfaction (dissatisfaction of any of them) verifies the presence of usual (exotic) fluid. They are, in fact, linear combination of different physical determinants characterizing the interior of a compact model. The influence of an electromagnetic field leads these bounds to the following

$$\begin{aligned}
\bar{\rho} + \frac{q^2}{8\pi r^4} &\geq 0, & \bar{\rho} + \bar{P}_r &\geq 0, \\
\bar{\rho} + \bar{P}_t + \frac{q^2}{4\pi r^4} &\geq 0, & \bar{\rho} - \bar{P}_r + \frac{q^2}{4\pi r^4} &\geq 0, \\
\bar{\rho} - \bar{P}_t &\geq 0, & \bar{\rho} + \bar{P}_r + 2\bar{P}_t + \frac{q^2}{4\pi r^4} &\geq 0.
\end{aligned} \tag{78}$$

The most important phenomenon in the study of compact stars is that how long these structures remain stable during evolutionary changes. Therefore, we employ sound speed criteria to check the stable regions of our proposed models. The sound speed is defined as the variation in pressure against the variation in the density, i.e., $v_s^2 = \frac{dP}{d\rho}$. Since the current scenario contains effective variables as well as anisotropic fluid, the sound speed is classified in radial ($v_{sr}^2 = \frac{d\bar{P}_r}{d\bar{\rho}}$) and tangential ($v_{st}^2 = \frac{d\bar{P}_t}{d\bar{\rho}}$) directions. Their acceptable ranges were reported as $0 < v_{sr}^2, v_{st}^2 < 1$ to get a stable system [52]. Herrera then studied the occurrence of cracking in compact stars and combined the above both factors in a single framework, and suggested that a stable interior must fulfill $0 < |v_{st}^2 - v_{sr}^2| < 1$ [53]. Another phenomenon in this regard is the adiabatic index that plays a key role in determining the nature of pressure. According to the research [54], if the adiabatic index is greater than $\frac{4}{3}$, a perturbation that compresses the star will lead to an increase in pressure. This increment in pressure resists the compression and ultimately contributes to the star's stability. On the other hand, if the adiabatic index is less than the above-mentioned limit, compression will cause a decrease in pressure, leading to further compression and overall instability of the star occurs. Mathematically, it is defined as

$$\bar{\Gamma} = \frac{\bar{\rho} + \bar{P}_r}{\bar{P}_r} \left(\frac{d\bar{P}_r}{d\bar{\rho}} \right) = \frac{\bar{\rho} + \bar{P}_r}{\bar{P}_r} (v_{sr}^2). \tag{79}$$

We now discuss physical interpretation of the obtained models by plotting the corresponding deformation functions, extended g_{rr} metric potentials, physical parameters and several other factors. We adopt four different values of the decoupling parameter such as $\omega = 0.25, 0.5, 0.75$ and 1. Further, the

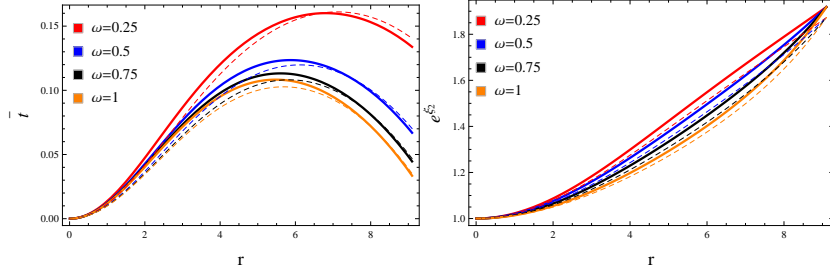


Figure 1: Deformation function (43) and deformed g_{rr} metric potential (44) corresponding to $\mathcal{Q} = 0.1$ (solid) and 0.8 (dashed) for the solution generated by $\bar{\Pi} = 0$.

effect of charge on developed models is also checked by taking $\mathcal{Q} = 0.1, 0.8$ and $\xi_5 = -0.001$ into account. The first model corresponds to $\bar{\Pi} = 0$ is investigated in the following. Figure 1 (left) exhibits the deformation function (43) that disappears at $r = 0$, increasing initially and then decreasing towards the spherical boundary. The right plot indicates that the corresponding radial coefficient (44) shows a non-singular increasing trend, and it takes the same values at the core as well as hypersurface for all parametric values. The physical determinants must be maximum in the center of a star and decrease towards its boundary, as indicated by Figure 2. The upper left graph shows that the energy density decreases with a rise in the decoupling parameter and charge near the center, and vice versa near the boundary. The tangential pressure, on the other hand, behaves opposite to the energy density (lower left). Further, the spherical junction possesses only the tangential pressure whereas the radial component becomes null at that point. As far as the anisotropy is concerned, it becomes zero at the core (as radial and tangential pressures are equal) and increases outwards (lower right). It must be mentioned that the above-described behavior of anisotropy is just for $\omega = 0.25, 0.5$ and 0.75 . However, this factor vanishes throughout for $\omega = 1$, leading to the isotropic interior.

The mass function is plotted in Figure 3 (upper left) that becomes zero at $r = 0$ and possesses an increasing trend outwards. It is observed that the anisotropic interior is dense as compared to the isotropic analog for both values of the electric charge. The upper right and lower graphs are in agreement with the required criteria of compactness and redshift. Tables 1 and 2 provide the numerical values of these quantities. Further, we notice that the

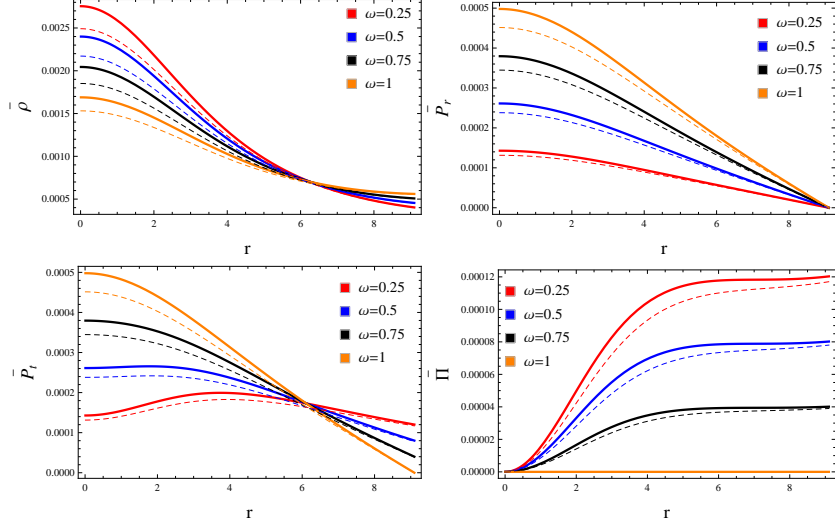


Figure 2: Physical variables corresponding to $Q = 0.1$ (solid) and 0.8 (dashed) for the solution generated by $\bar{\Pi} = 0$.

density and both pressures are positively definite everywhere, thus only the dominant energy bounds like $\bar{\rho} - \bar{P}_r + \frac{q_2^2}{4\pi r^4} \geq 0$ and $\bar{\rho} - \bar{P}_t \geq 0$ are plotted in Figure 4, making sure the existence of viable resulting model.

Table 1: Values of physical parameters for a compact star $4U\ 1820 - 30$ with $Q = 0.1$ corresponding to the solution generated by $\bar{\Pi} = 0$.

ω	ρ_c (gm/cm^3)	ρ_s (gm/cm^3)	P_c ($dyne/cm^2$)	τ_s	z_s
0.25	3.6844×10^{15}	5.4369×10^{14}	1.7267×10^{35}	0.247	0.406
0.5	3.1988×10^{15}	5.9748×10^{14}	3.1095×10^{35}	0.247	0.406
0.75	2.7332×10^{15}	6.6932×10^{14}	4.5608×10^{35}	0.247	0.406
1	2.2663×10^{15}	7.5909×10^{14}	5.9772×10^{35}	0.247	0.406

Table 2: Values of physical parameters for a compact star $4U\ 1820 - 30$ with $Q = 0.8$ corresponding to the solution generated by $\bar{\Pi} = 0$.

ω	ρ_c (gm/cm^3)	ρ_s (gm/cm^3)	P_c ($dyne/cm^2$)	τ_s	z_s
0.25	3.3245×10^{15}	5.4289×10^{14}	1.5535×10^{35}	0.238	0.384
0.5	2.8937×10^{15}	6.1755×10^{14}	2.8329×10^{35}	0.238	0.384
0.75	2.4817×10^{15}	6.7762×10^{14}	4.1808×10^{35}	0.238	0.384
1	2.0509×10^{15}	7.4932×10^{14}	5.4241×10^{35}	0.238	0.384

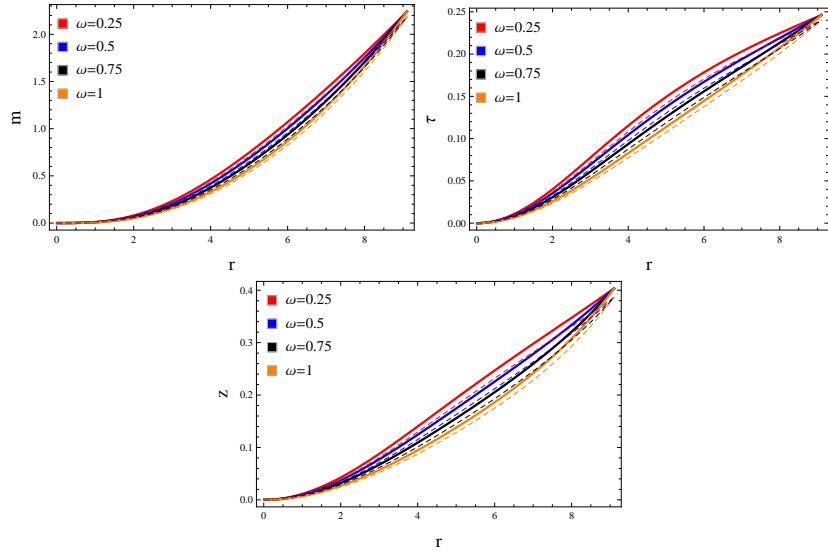


Figure 3: Different factors corresponding to $Q = 0.1$ (solid) and 0.8 (dashed) for the solution generated by $\bar{\Pi} = 0$.

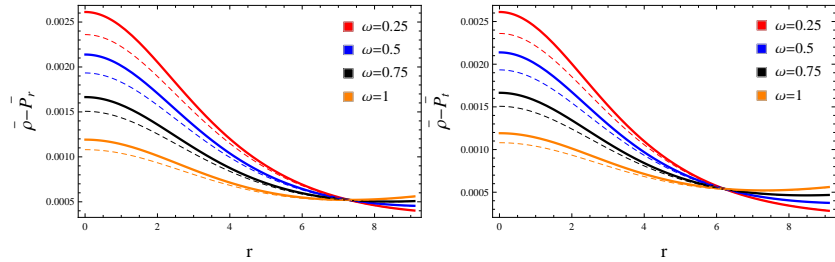


Figure 4: Dominant energy bounds corresponding to $Q = 0.1$ (solid) and 0.8 (dashed) for the solution generated by $\bar{\Pi} = 0$.

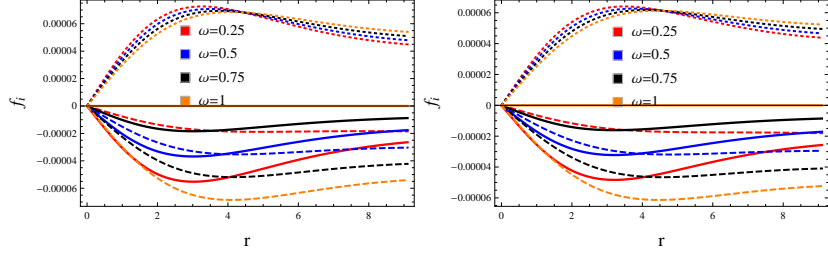


Figure 5: Different forces including f_a (solid), f_h (dashed) and f_w (dotted) corresponding to $Q = 0.1$ (left) and 0.8 (right) for the solution generated by $\bar{\Pi} = 0$.

Different forces in TOV equation (30) are plotted in Figure 5 and we find that the resulting solution is in the hydrostatic equilibrium. Figure 6 determines the stability analysis by means of sound speeds and adiabatic index. The radial and tangential sound speed components alongside the lower right plot provide that our model is stable for all parametric values except $\omega = 1$. This implies that the isotropic analog is no more physically relevant in contrast with [44]. The scalars (54) and (67) describing the complexity of compact sources are plotted in Figure 7 which decrease and increase with the increment in ω , respectively. However, the first scalar increases throughout with the radial coordinate while the other factor initially increases and then decreases towards the spherical junction. Further, the reduction in the complexity is observed in the presence of charge, making it interesting to be studied.

The deformation functions and their corresponding radial metric components for the constraints $Y_{TF}^Z = 0$ and $\bar{Y}_{TF} = 0$ are pictured in Figures 8 and 9, respectively, showing an acceptable (increasing and free from singularity) trend. The solution for the later constraint is now physically interpreted in the following for the same parametric choices. Figure 10 demonstrates the profile of the matter triplet (presented in Eqs.(74)-(76)) along with the corresponding pressure anisotropy. The density and pressure components exhibit the same behavior as we have already observed corresponding to the first model. However, the anisotropy initially becomes zero at the core, decreases outwards against r and then again possesses increasing behavior. Further, the less value of charge makes the structure more anisotropic (lower right). Figure 11 (upper left) points out that there is a slight difference between the spherical mass function for different values of ω . Moreover, other criteria

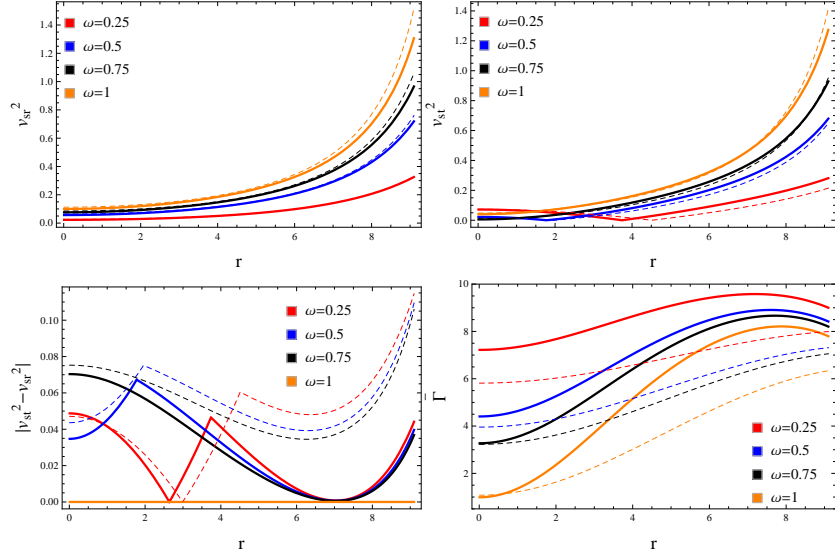


Figure 6: Radial/tangential speeds of sound, $|v_{st}^2 - v_{sr}^2|$ and adiabatic index corresponding to $Q = 0.1$ (solid) and 0.8 (dashed) for the solution generated by $\bar{\Pi} = 0$.

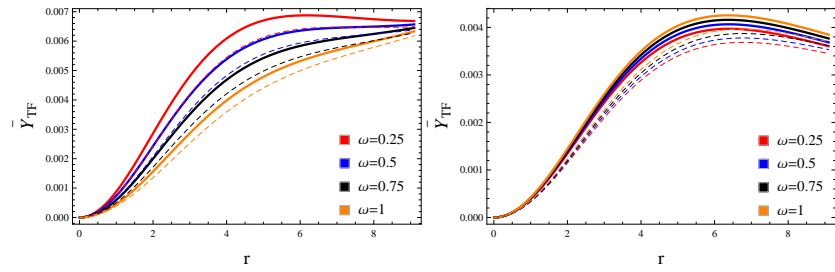


Figure 7: Complexity factors (54) and (67) corresponding to $Q = 0.1$ (solid) and 0.8 (dashed).

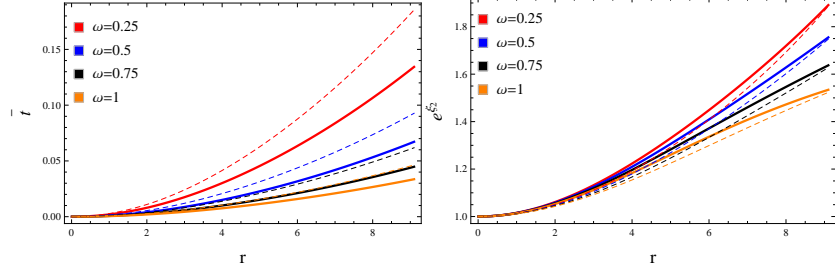


Figure 8: Deformation function (64) and deformed g_{rr} metric potential (66) corresponding to $Q = 0.1$ (solid) and 0.8 (dashed) for the solution generated by $Y_{TF}^Z = 0$.

for redshift and compactness are also fulfilled. The numerical values of these physical factors are presented in Tables 3 and 4. The acceptable behavior of energy conditions ensures a viable resulting model that can be seen in Figure 12. The hydrostatic equilibrium condition for this model is verified in Figure 13 for all parametric values. The upper left and lower right plots of Figure 14 reveal that the developed solution is stable for every parametric choice except $\omega = 1$.

Table 3: Values of physical parameters for a compact star $4U\ 1820 - 30$ with $Q = 0.1$ corresponding to the solution generated by $Y_{TF}^Z = 0$.

ω	ρ_c (gm/cm^3)	ρ_s (gm/cm^3)	P_c ($dyne/cm^2$)	τ_s	z_s
0.25	2.3426×10^{15}	6.6624×10^{14}	5.7295×10^{35}	0.248	0.404
0.5	2.1472×10^{15}	6.8417×10^{14}	6.2935×10^{35}	0.248	0.404
0.75	1.9425×10^{15}	7.2096×10^{14}	6.9007×10^{35}	0.248	0.404
1	1.7512×10^{15}	7.5401×10^{14}	7.5079×10^{35}	0.248	0.404

Table 4: Values of physical parameters for a compact star $4U\ 1820 - 30$ with $Q = 0.8$ corresponding to the solution generated by $Y_{TF}^Z = 0$.

ω	ρ_c (gm/cm^3)	ρ_s (gm/cm^3)	P_c ($dyne/cm^2$)	τ_s	z_s
0.25	2.1606×10^{15}	6.5193×10^{14}	5.0791×10^{35}	0.239	0.386
0.5	1.9773×10^{15}	6.8257×10^{14}	5.5997×10^{35}	0.239	0.386
0.75	1.8088×10^{15}	7.1013×10^{14}	6.1636×10^{35}	0.239	0.386
1	1.6322×10^{15}	7.4183×10^{14}	6.7275×10^{35}	0.239	0.386

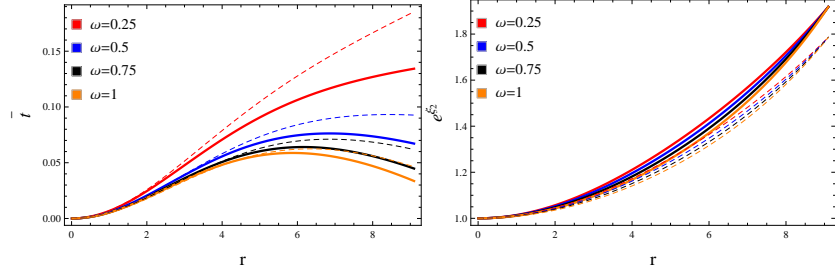


Figure 9: Deformation function (72) and deformed g_{rr} metric potential (73) corresponding to $Q = 0.1$ (solid) and 0.8 (dashed) for the solution generated by $\tilde{Y}_{TF} = 0$.

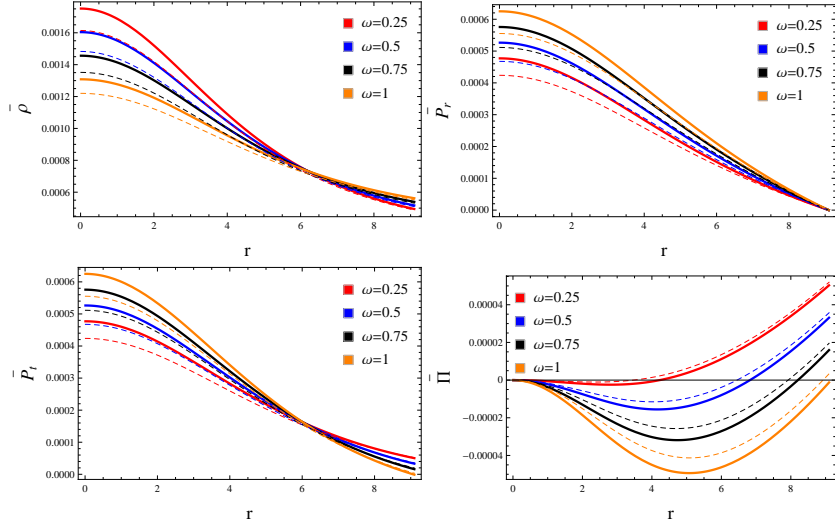


Figure 10: Physical variables corresponding to $Q = 0.1$ (solid) and 0.8 (dashed) for the solution generated by $\tilde{Y}_{TF} = 0$.

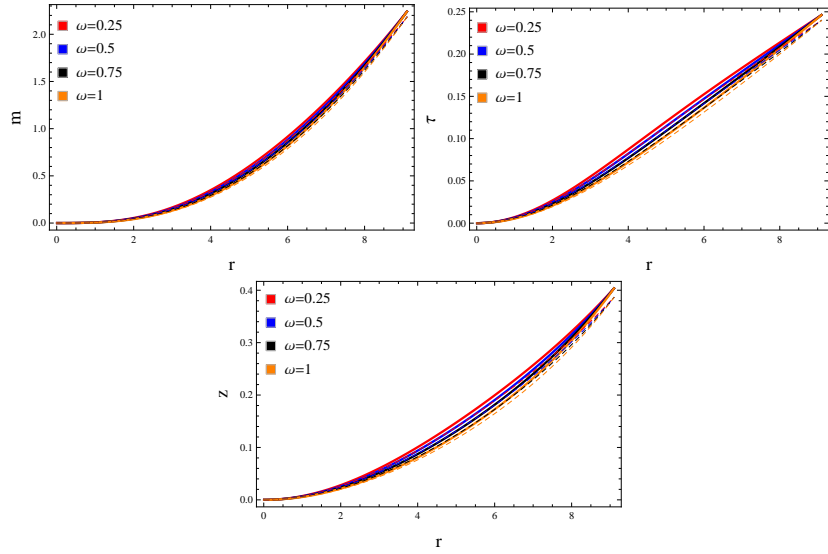


Figure 11: Different factors corresponding to $Q = 0.1$ (solid) and 0.8 (dashed) for the solution generated by $\bar{Y}_{TF} = 0$.

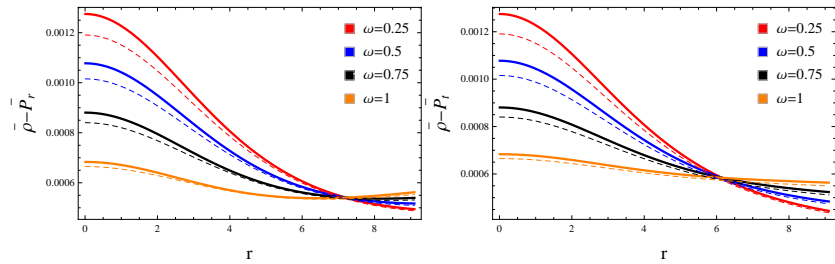


Figure 12: Dominant energy bounds corresponding to $Q = 0.1$ (solid) and 0.8 (dashed) for the solution generated by $\bar{Y}_{TF} = 0$.

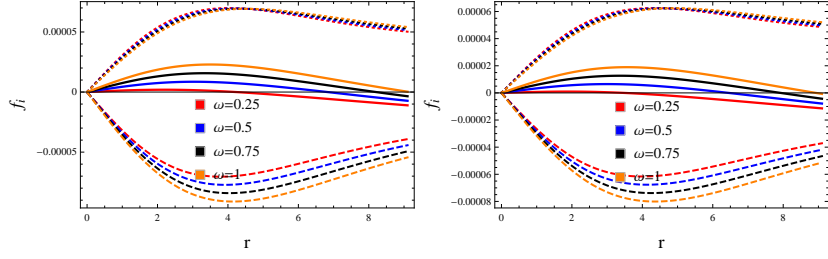


Figure 13: Different forces including f_a (solid), f_h (dashed) and f_w (dotted) corresponding to $Q = 0.1$ (left) and 0.8 (right) for the solution generated by $\bar{Y}_{TF} = 0$.

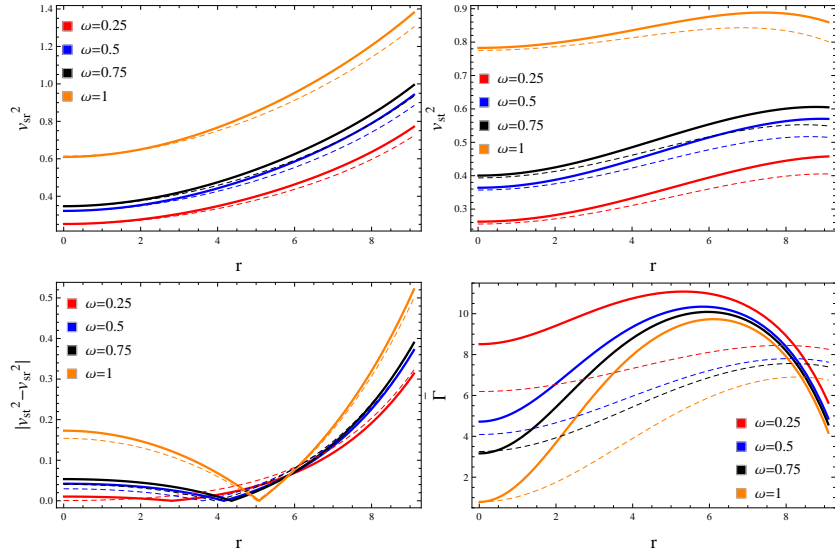


Figure 14: Radial/tangential speeds of sound, $|v_{st}^2 - v_{sr}^2|$ and adiabatic index corresponding to $Q = 0.1$ (solid) and 0.8 (dashed) for the solution generated by $\bar{Y}_{TF} = 0$.

7 Conclusions

This paper investigates the nature of two different anisotropic spherically symmetric solutions under the impact of an electromagnetic field through a systematic scheme, referred as the gravitational decoupling. For this, we have considered a static sphere configured with the anisotropic interior as a seed source and added another fluid distribution. We have then developed the field equations possessing both matter sources, however, it was hard enough to find their solution due to the increment in unknowns. This problem was handled by applying the MGD technique that divides these equations into two independent sets. We have observed that charge contributes only in the first set characterizing the initial fluid source. Since we need to find multiple solutions, thus we have adopted some specific metric ansatz as

$$\xi_1(r) = \ln \left\{ C_2^2 \left(1 + \frac{r^2}{C_1^2} \right) \right\}, \quad \xi_4(r) = e^{-\xi_2(r)} = \frac{C_1^2 + r^2}{C_1^2 + 3r^2},$$

and Tolman IV components to deal with the first set. These spacetimes contain an unknown triplet (C_1, C_2, C_3) that needed to be calculated. To do this, we have taken the Reissner-Nordström metric and matched it with the interior geometry at the spherical junction that made the above triplet known. As for the other set (20)-(22) is concerned, we have assumed different constraints on the additional field $Z_{\lambda\chi}$ to determine the deformation function, ultimately resulting in different solutions. The first model was based on the assumption that we can convert the anisotropic system to an isotropic interior for a specific parametric value, i.e., $\omega = 1$. Moreover, the total fluid configuration was reviewed to be free from complexity, leading to the second model.

We have explored the graphical nature of the developed models by adopting multiple values of charge and the decoupling parameter to observe how these models behave in the considered scenario. Further, we have assumed an interior charge in a particular form involving a constant whose value has been suggested as $\xi_5 = -0.001$ [35] to get acceptable results. We have adopted different values of this constant and deduced that only the suggested value provided physically relevant properties of a compact star. In addition, we have calculated the values of D_1 and D_3 by taking into account the vanishing radial pressure at the spherical boundary. Different parameters such as the deformation function, extended radial metric component, the matter triplet (defined in (46)-(48) and (74)-(76)), anisotropic factors, the mass function,

redshift, compactness and the viability conditions have been checked for both solutions and found an acceptable profile. We have also observed that the resulting anisotropic interior corresponding to $\bar{Y}_{TF} = 0$ becomes less dense for every ω as compared to the other model. Figures **5** and **13** show that both the developed solutions fulfil the hydrostatic equilibrium condition for every parametric choice.

The stability of these structures has also been studied through the sound speed and adiabatic index so that we can check whether the MGD strategy on the charged interiors results in acceptable results or not. Both these criteria revealed that our resulting solutions are stable everywhere for all values of ω and charge except $\omega = 1$, contradicting the uncharged framework [43] as well as Brans-Dicke theory [44] (Figures **6** and **14**). Sharif and Sadiq [30] formulated two new decoupled charged anisotropic models through two constraints. They analyzed the effects of both decoupling parameter and an electromagnetic field on them, and found them unstable for the considered parametric values. Hence, we can say that the MGD approach along with the complexity of a compact model produce more efficient results. To compare our results with the observational data, we have adopted a compact star $4U\ 1820 - 30$ along with its estimated radius and mass. Tables **1-4** portray the numerical values of the central and surface density for all chosen values of the decoupling parameter and charge. We have found them of order 10^{14} or 10^{15} , which is sufficiently high and consistent with compact stars. We have also calculated the mass of a considered compact star as

- $\mathcal{M} = 1.531\mathcal{M}_{\odot}$ and $1.499\mathcal{M}_{\odot}$ for $\mathcal{Q} = 0.1$ and 0.8 , respectively, corresponding to the model generated by $\bar{\Pi} = 0$,
- $\mathcal{M} = 1.538\mathcal{M}_{\odot}$ and $1.501\mathcal{M}_{\odot}$ for $\mathcal{Q} = 0.1$ and 0.8 , respectively, corresponding to the model generated by $\bar{Y}_{TF} = 0$.

Hence, it is observed that the lower values of charge produce a best fit to the existing data. It is worth mentioning that our results reduce to [43] for the vanishing charge.

Data Availability Statement: This manuscript has no associated data.

References

- [1] Schwarzschild, K.: Sitz. Deut. Akad. Wiss Berlin Kl. Math. Phys. **1916**(1916)189.

- [2] Schwarzschild, K.: Sitz. Deut. Akad. Wiss Berlin Kl. Math. Phys. **24**(1916)424.
- [3] Ovalle, J.: Mod. Phys. Lett. A **23**(2008)3247.
- [4] Ovalle, J. and Linares, F.: Phys. Rev. D **88**(2013)104026.
- [5] Ovalle, J.: Int. J. Mod. Phys. D **18**(2009)837.
- [6] Ovalle, J.: Mod. Phys. Lett. A **25**(2010)3323.
- [7] Sharif, M. and Naseer, T.: Chin. J. Phys. **73**(2021)179; Eur. Phys. J. Plus **137**(2022)1304; Gen. Relativ. Gravit. **55**(2023)87; Naseer, T. and Sharif, M.: Universe **8**(2022)62; Fortschr. Phys. **71**(2023)2300004.
- [8] Casadio, R. and Ovalle, J.: Phys. Lett. B **715**(2012)251.
- [9] Casadio, R. and Ovalle, J.: Gen. Rel. Grav. **46**(2014)1669
- [10] Ovalle, J., Linares, F., Pasqua, A. and Sotomayor, A.: Class. Quantum Grav. **30**(2013)175019.
- [11] Casadio, R. and Harms, B.: Phys. Rev. D **64**(2001)024016.
- [12] da Rocha, R. and Hoff da Silva, J.M.: Phys. Rev. D **85**(2012)046009.
- [13] Bazeia, D., Hoff da Silva, J.M. and da Rocha, R.: Phys. Lett. B **721**(2013)306.
- [14] da Rocha, R., Piloyan, A. and Kuerten, A.M.: Class. Quantum Grav. **30**(2013)045014.
- [15] Herrera-Aguilar, A., Kuerten, A.M. and da Rocha, R.: Adv. High Energy Phys. **2015**(2015)359268.
- [16] Casadio, R., Ovalle, J. and Da Rocha, R.: Class. Quantum Grav. **32**(2015)215020.
- [17] Jeans, J.: Mon. Not. R. Astron. Soc. **82**(1922)122.
- [18] Ruderman, M.: Annu. Rev. Astron. Astrophys. **10**(1972)427.
- [19] Yazadjiev, S.S.: Phys. Rev. D **85**(2012)044030.

- [20] Cardall, C.Y., Prakash, M. and Lattimer, J.M.: *Astrophys. J.* **554**(2001)322.
- [21] Ciolfi, R., Ferrari, V. and Gualtieri, L.: *Mon. Not. R. Astron. Soc.* **406**(2010)2540.
- [22] Friebe, J. and Rezzolla, L.: *Mon. Not. R. Astron. Soc.* **427**(2012)3406.
- [23] Sawyer, R.F.: *Phys. Rev. Lett.* **29**(1972)382.
- [24] Canuto, V. *Annu. Rev. Astron. Astrophys.* **12**(1974)167.
- [25] Heiselberg, H. and Hjorth-Jensen, M.: *Phys. Rep.* **328**(2000)237.
- [26] Ovalle, J. et al.: *Eur. Phys. J. C* **78**(2018)960.
- [27] Estrada, M. and Tello-Ortiz, F.: *Eur. Phys. J. Plus* **133**(2018)453.
- [28] Gabbanelli, L., Rincón, Á. and Rubio, C.: *Eur. Phys. J. C* **78**(2018)370.
- [29] Hens, S. and Stuchlík, Z.: *Eur. Phys. J. C* **79**(2019)834.
- [30] Sharif, M. and Sadiq, S.: *Eur. Phys. J. C* **78**(2018)410.
- [31] Sharif, M. and Saba, S.: *Eur. Phys. J. C* **78**(2018)921; Sharif, M. and Waseem, A.: *Ann. Phys.* **405**(2019)14; Sharif, M. and Majid, A.: *Chin. J. Phys.* **68**(2020)406.
- [32] Sharif, M. and Naseer, T.: *Phys. Scr.* **97**(2022)055004; *ibid.* **97**(2022)125016; *Int. J. Mod. Phys. D* **31**(2022)2240017; *Fortschr. Phys.* **71**(2023)2200147.
- [33] Bekenstein, J.D.: *Phys. Rev. D* **4**(1971)2185.
- [34] Esculpi, M. and Aloma, E.: *Eur. Phys. J. C* **67**(2010)521.
- [35] de Felice, F., Yu, Y.Q. and Fang, J.: *Mon. Not. R. Astron. Soc.* **277**(1995)L17.
- [36] de Felice, F., Liu, S.M. and Yu, Y.Q.: *Class. Quantum Gravit.* **16**(1999)2669.
- [37] Maurya, S.K. et al.: *Eur. Phys. J. C* **75**(2015)389.

- [38] Herrera, L.: Phys. Rev. D **97**(2018)044010.
- [39] Herrera, L., Di Prisco, A. and Ospino, J.: Phys. Rev. D **98**(2018)104059.
- [40] Yousaf, Z., Bhatti, M.Z. and Naseer, T.: Eur. Phys. J. Plus **135**(2020)353; Phys. Dark Universe **28**(2020)100535; Int. J. Mod. Phys. D **29**(2020)2050061; Ann. Phys. **420**(2020)168267.
- [41] Yousaf, Z. et al.: Phys. Dark Universe **29**(2020)100581; Yousaf, Z. et al.: Mon. Not. R. Astron. Soc. **495**(2020)4334; Sharif, M. and Naseer, T.: Chin. J. Phys. **77**(2022)2655; Eur. Phys. J. Plus **137**(2022)947.
- [42] Carrasco-Hidalgo, M. and Contreras, E.: Eur. Phys. J. C **81**(2021)757; Andrade, J. and Contreras, E.: Eur. Phys. J. C **81**(2021)889.
- [43] Casadio, R. et al.: Eur. Phys. J. C **79**(2019)826.
- [44] Sharif, M. and Majid, A.: Eur. Phys. J. Plus **137**(2022)114.
- [45] Maurya, S.K. and Nag, R.: Eur. Phys. J. C **82**(2022)48; Maurya, S.K. et al.: Eur. Phys. J. C **82**(2022)100.
- [46] Arias, C. et al.: Ann. Phys. **436**(2022)168671; Sharif, M. and Naseer, T.: Ann. Phys. **453**(2023)169311.
- [47] Sharif, M. and Naseer, T.: Class. Quantum Gravit. **40**(2023)035009.
- [48] Einstein, A.: Ann. Math. **40**(1939)922.
- [49] Güver, T., Wroblewski, P., Camarota, L. and Özel, F.: Astrophys. J. **719**(2010)1807.
- [50] Buchdahl, H.A.: Phys. Rev. **116**(1959)1027.
- [51] Ivanov, B.V.: Phys. Rev. D **65**(2002)104011.
- [52] Abreu, H., Hernandez, H. and Nunez, L.A.: Class. Quantum Gravit. **24**(2007)4631.
- [53] Herrera, L.: Phys. Lett. A **165**(1992)206.
- [54] Heintzmann, H. and Hillebrandt, W.: Astron. Astrophys. **38**(1975)51.